Evaluation of wave-frequency motions extraction from dynamic positioning measurements using the empirical mode decomposition

Paula B. Garcia-Rosa
Department of Electric Power Engineering
Norwegian University of Science and Technology
Trondheim, Norway
p.b.garcia-rosa@ieee.org

Astrid H. Brodtkorb
Department of Marine Technology
Norwegian University of Science and Technology
Trondheim, Norway
astrid.h.brodtkorb@ntnu.no

Asgeir J. Sørensen
Department of Marine Technology
Norwegian University of Science and Technology
Trondheim, Norway
asgeir.sorensen@ntnu.no

Marta Molinas
Department of Engineering Cybernetics
Norwegian University of Science and Technology
Trondheim, Norway
marta.molinas@ntnu.no

***Abstract*—For dynamic positioning operations, high-frequency wave induced motions cause excessive control action, and consequently additional power consumption and wear of actuators in the propulsion system. Thus, such operations require the control of only low-frequency motions, which is achieved by proper filtering of high-frequency motions. This study investigates the use of the empirical mode decomposition (EMD) method for wave filtering purposes. EMD is a data-driven method that decomposes an oscillatory waveform into a number of modes from the highest to the lowest frequency. The decomposition process in the standard EMD algorithm relies on repetitive iterations through the entire data span, which is impractical for wave filtering in real-time applications. Thus, an online EMD algorithm is also considered. The online decomposition process features a time lag, and measurements of the ship motions have to be taken at a point ahead of the center of gravity so that high-frequency motions are estimated in advance. In this study, the performance of both standard and online EMD algorithms, in terms of wave filtering and control efforts, is evaluated through a comparison with a nonlinear passive observer (NPO). Furthermore, the time lag of the online EMD is also of interest, as it indicates the required prediction time window. Simulation results with a simple maneuver of a vessel in moderate, and calm seas, show that the control action with wave filtering from the online EMD can be up to 40% lower than with wave filtering from NPO.**

***Index Terms*—wave filtering, dynamic positioning, empirical mode decomposition**

I. Introduction

In most ship applications, the oscillatory motion due to first-order wave forces and moments should not enter the control loop, as it causes unnecessary tear and wear on the machinery and thrusters, and consequently, increases fuel consumption. Such an oscillatory motion is caused by waves in the frequency range [1]:

$$0.05 < f_0 < 0.2 \qquad \text{(Hz)}\,. \tag{1}$$

The ship is also subject to wave drift forces that are caused by second-order wave disturbances and induce nonzero slowly-varying motions. However, second-order wave drift forces can be counteracted by the motion-control loop [1], [2].

In order to avoid high-frequency wave induced motions, which cause excessive control action, proper filtering of state variables must be performed by using wave filtering techniques. In this study, the focus is on wave filtering for dynamic positioning (DP) systems. In this framework, a number of studies have developed wave filtering techniques based on conventional filter design, and state estimation methods, see, e.g., [2]–[7]. Techniques based on state estimation consist of using a wave-induced motion model and an observer to separate the ship position and heading into wave-frequency (WF) motions (i.e., the high-frequency wave induced motions) and low-frequency (LF) motions [2], [5].

A non-model based approach is considered here, where a scheme based on the empirical mode decomposition (EMD) method is proposed to extract the first-order oscillatory motions from the ship position and heading measurements. EMD is a data-driven method with an adaptive basis that relies on the local characteristic time-scale of an oscillatory waveform. The method decomposes a waveform into a number of intrinsic mode functions (IMFs) from the highest to the lowest frequency modes, and a residue, which can be either the mean trend or a constant [8]. An IMF is defined as a symmetric signal with respect to the local zero mean, and with numbers of zero crossings and extrema that differ at most by one. Such a signal satisfies the necessary conditions for a physically meaningful interpretation of instantaneous frequency obtained from the Hilbert transform [8].

The aim of this paper is to evaluate the performance of the EMD method for wave filtering purposes in DP systems.

Simulation results present a comparison of both wave filtering and control efforts for the case when wave-frequency motions are filtered by EMD with the case when a nonlinear passive observer (NPO) [2] is used.

Moreover, the decomposition process in the standard EMD algorithm relies on repetitive iterations through the entire data span, which would cause excessively long delays, impractical for wave filtering purposes in real-time applications. Thus, an online EMD algorithm based on a sliding window and stitching procedure [9] is also considered in this study. Ultimately, the WF motions feature a time lag due to the online decomposition process, and then, measurements of the ship position and heading have to be taken at a point ahead of the center of gravity (CG) so that WF motions are estimated in advance. The time lag of the EMD online indicates the required prediction time window.

Both standard and online EMD algorithms are adopted in this study. Therefore, the wave-frequency motions obtained with the online EMD can be verified through a comparison with results obtained with the standard EMD.

II. Mathematical Models for DP systems and wave filtering

DP mathematical models can be formulated by using either a low-fidelity model, which is a simplified model with the main physical properties of the process, or a high-fidelity model, which represents a more comprehensive description of the process and is used for simulating the real plant dynamics [10]. Here, we describe the low-fidelity model used in the NPO formulation.

A. Modeling of DP vessels

Ship operations such as station-keeping and low-speed maneuvering rely on feedback information from position and heading measurements. Such measurements are used in a motion-control system operating in three planar degrees of freedom, i.e., surge, sway and heading [5]. The models described here consider three degrees of freedom only.

Two reference frames can be adopted to describe the motion of a ship, i.e., the local geographical Earth-fixed frame and the body-fixed frame. Furthermore, the total motion of the vessel ($\mathbf{y} \in \mathbb{R}^3$) can be calculated as the superposition of low-frequency motions ($\boldsymbol{\eta} \in \mathbb{R}^3$) and wave-frequency motions ($\boldsymbol{\eta}_w \in \mathbb{R}^3$). For control system design, the model of the vessel can be expressed as [10]:

$$\begin{aligned}
\dot{\boldsymbol{\xi}} &= \mathbf{A}_w \boldsymbol{\xi} + \mathbf{E}_w \mathbf{w}_w \,, && (2)\\
\boldsymbol{\eta}_w &= \mathbf{C}_w \boldsymbol{\xi} \,, && (3)\\
\dot{\boldsymbol{\eta}} &= \mathbf{R}(\psi)\, \boldsymbol{\nu} \,, && (4)\\
\mathbf{M}\dot{\boldsymbol{\nu}} &= -\mathbf{D}\boldsymbol{\nu} + \mathbf{R}^T(\psi)\mathbf{b} + \boldsymbol{\tau}_c \,, && (5)\\
\dot{\mathbf{b}} &= -\mathbf{T}_b^{-1}\mathbf{b} + \mathbf{E}_b \mathbf{w}_b \,, && (6)\\
\mathbf{y} &= \boldsymbol{\eta} + \boldsymbol{\eta}_w + \mathbf{w}_y \,, && (7)
\end{aligned}$$

where $\mathbf{R}(\psi)$ is the rotation matrix,

$$\mathbf{R}(\psi) = \begin{bmatrix} \cos\psi & -\sin\psi & 0 \\ \sin\psi & \cos\psi & 0 \\ 0 & 0 & 1 \end{bmatrix}, \qquad (8)$$

the LF position-orientation vector $\boldsymbol{\eta} = [\mathcal{N}, \mathcal{E}, \psi]^T$ represents the north, east $(\mathcal{N}, \mathcal{E})$ positions relative to the Earth-fixed frame and the heading angle (ψ) relative to the north, whereas the vector $\boldsymbol{\eta}_w = [\mathcal{N}_w, \mathcal{E}_w, \psi_w]^T$ represents the WF north, east positions and heading, and $\mathbf{w}_y \in \mathbb{R}^3$ is a measurement noise vector.

The velocity vector $\boldsymbol{\nu} = [u, v, r]^T$ represents the surge, sway velocities (u, v) and the yaw rate (r), $\mathbf{M} \in \mathbb{R}^{3\times3}$ is the inertia matrix including the rigid-body mass and hydrodynamic added mass matrices, $\mathbf{D} \in \mathbb{R}^{3\times3}$ is the linear damping matrix, $\boldsymbol{\tau}_c = [\tau_{\text{surge}}, \tau_{\text{sway}}, \tau_{\text{yaw}}]^T$ is the control vector in the body-frame obtained from a nonlinear PID controller [11], and $\mathbf{b} \in \mathbb{R}^3$ is a bias vector term that accounts for slowly-varying disturbances and unmodeled dynamics. In the bias model (6), $\mathbf{T}_b \in \mathbb{R}^{3\times3}$ is a diagonal matrix of bias constants, and $\mathbf{E}_b \in \mathbb{R}^{3\times3}$ is a diagonal matrix that weights the amplitudes of the white noise vector $\mathbf{w}_b \in \mathbb{R}^3$.

The WF model (2)-(3) is based on linear approximations of wave spectrum descriptions [1]. For each degree of freedom $i = \{1, 2, 3\}$, the state-space model represents a 2nd-order noise-driven damped oscillator with relative damping ratio ζ_i and angular frequency ω_{oi} defined as the peak frequency of the wave spectrum. The matrices $\mathbf{A}_w$, $\mathbf{C}_w$, $\mathbf{E}_w$ are given by

$$\mathbf{A}_w = \begin{bmatrix} \mathbf{0}_{3\times3} & \mathbf{I}_{3\times3} \\ -\boldsymbol{\Omega}^2 & -2\boldsymbol{\Lambda}\boldsymbol{\Omega} \end{bmatrix}, \; \mathbf{C}_w = \begin{bmatrix} \mathbf{0}_{3\times3} & \mathbf{I}_{3\times3} \end{bmatrix}, \; \mathbf{E}_w = \begin{bmatrix} \mathbf{0}_{3\times3} \\ \mathbf{E}_w \end{bmatrix},$$

where $\boldsymbol{\Omega} = \text{diag}\{\omega_{o1}, \omega_{o2}, \omega_{o3}\}$, $\boldsymbol{\Lambda} = \text{diag}\{\zeta_1, \zeta_2, \zeta_3\}$, $\mathbf{E}_{w2} = \text{diag}\{\epsilon_{w1}, \epsilon_{w2}, \epsilon_{w3}\}$, and ϵ_{wi} is a parameter related to the wave intensity [2].

B. Model-based Observer

The nonlinear passive observer considered here is based on the model (2)-(7), which is a simplified model of the vessel dynamics. The observer inputs are the measurements of ship position and heading ($\mathbf{y}$) and the control input vector ($\boldsymbol{\tau}_c$). The model-based observer is given by [2]

$$\begin{aligned}
\dot{\hat{\boldsymbol{\xi}}} &= \mathbf{A}_w \hat{\boldsymbol{\xi}} + \mathbf{K}_1 \tilde{\mathbf{y}} \,, && (9)\\
\dot{\hat{\boldsymbol{\eta}}} &= \mathbf{R}(\psi_y)\, \hat{\boldsymbol{\nu}} + \mathbf{K}_2 \tilde{\mathbf{y}} \,, && (10)\\
\dot{\hat{\mathbf{b}}} &= -\mathbf{T}_b^{-1}\hat{\mathbf{b}} + \mathbf{K}_3 \tilde{\mathbf{y}} \,, && (11)\\
\mathbf{M}\dot{\hat{\boldsymbol{\nu}}} &= -\mathbf{D}\hat{\boldsymbol{\nu}} + \mathbf{R}^T(\psi_y)\hat{\mathbf{b}} + \boldsymbol{\tau}_c + \mathbf{K}_4 \mathbf{R}^T(\psi_y)\tilde{\mathbf{y}} \,, && (12)\\
\hat{\mathbf{y}} &= \hat{\boldsymbol{\eta}} + \mathbf{C}_w \hat{\boldsymbol{\xi}} \,, && (13)
\end{aligned}$$

where ψ_y is the measured heading, $\hat{\boldsymbol{\xi}} \in \mathbb{R}^6$, $\{\hat{\boldsymbol{\eta}}, \hat{\boldsymbol{\nu}}, \hat{\mathbf{b}}\} \in \mathbb{R}^3$ are the state estimates, $\tilde{\mathbf{y}} = \mathbf{y} - \hat{\mathbf{y}}$ is the measurement estimation error, $\mathbf{K}_1 \in \mathbb{R}^{6\times3}$, $\mathbf{K}_2 \in \mathbb{R}^{3\times3}$, $\mathbf{K}_3 \in \mathbb{R}^{3\times3}$, and $\mathbf{K}_4 \in \mathbb{R}^{3\times3}$ are the observer gain matrices. To ensure passivity properties,

the observer gain matrices should have a diagonal structure [2] [11, Chapter 11]:

$$\mathbf{K}_1 = \begin{bmatrix} \text{diag}\{K_{11}, K_{12}, K_{13}\} \\ \text{diag}\{K'_{11}, K'_{12}, K'_{13}\} \end{bmatrix}, \mathbf{K}_2 = \text{diag}\{K_{21}, K_{22}, K_{23}\},$$
$$\mathbf{K}_3 = \text{diag}\{K_{31}, K_{32}, K_{33}\}, \quad \mathbf{K}_4 = \text{diag}\{K_{41}, K_{42}, K_{43}\},$$

where

$$\begin{aligned} K_{1i} &= -2\omega_{ci}(\zeta_{ni} - \zeta_i)\frac{\omega_{ci}}{\omega_{oi}}, \\ K'_{1i} &= 2\omega_{oi}(\zeta_{ni} - \zeta_i), \\ K_{2i} &= \omega_{ci}, \end{aligned}$$

and $1/T_{bi} \ll K_{3i}/K_{4i} < \omega_{oi} < \omega_{ci}$ for $i = \{1, 2, 3\}$. $\zeta_{ni} > \zeta_i$ determines the notch effect (wave filtering) and $\omega_{ci} > \omega_{oi}$ is the filter cutoff frequency. For more details on global stability properties of the observer and tuning of the gain matrices, see [2] [11, Chapter 11].

III. Wave Filtering using the EMD

The EMD determines the oscillation modes (IMFs) in the ship motions (surge, sway and heading) in an iterative way, where the fastest oscillations of each motion are extracted firstly, and the residuals of the signals are decomposed in the next iterations. For a degree of freedom i, the decomposition is summarized as:

$$\begin{aligned} y_i(t) &= c_{1,i}(t) + r_{1,i}(t) \\ &= c_{1,i}(t) + c_{2,i}(t) + r_{2,i}(t) \\ &= c_{1,i}(t) + c_{2,i}(t) + c_{3,i}(t) + r_{3,i}(t) \\ &= \sum_{n=1}^{N} c_{n,i}(t) + r_{N,i}(t), \end{aligned} \tag{14}$$

where $y_i(t)$ is the measured motion i, $c_{n,i}(t)$ is the n-th IMF component, and $r_{N,i}(t)$ is the final residue. The total number of extracted IMFs (N) can be defined, e.g., by the data length [12]. However, in this study the IMFs are defined as the high-frequency wave induced motions (WF motions) that have to be filtered out prior to the control loop. Thus, the frequency of each IMF has to be calculated in order to verify if it lies in the frequency range (1). Here, we simply use the information of the peak frequency of the IMF spectra. From (14), the WF motions are defined as:

$$\mathcal{N}_w(t) = \sum_{n=1}^{N} c_{n,1}(t), \tag{15}$$

$$\mathcal{E}_w(t) = \sum_{n=1}^{N} c_{n,2}(t), \tag{16}$$

$$\psi_w(t) = \sum_{n=1}^{N} c_{n,3}(t), \tag{17}$$

where N is defined according to the required wave filtering characteristics for the ship motion-control.

In order to estimate the WF motions using EMD (15)-(17), we assume that the ship is moving with low speed in opposite direction to the incident waves, and measurements of the ship position and heading are taken at a point ahead of the CG. Thus, the WF motions at the CG can be estimated in advance for wave filtering purposes.

A. Standard EMD

The EMD algorithm identifies local maxima and minima of the ship motion $y_i(t)$, and calculates upper and lower envelopes for such extrema using cubic splines. The mean values of the envelopes are used to decompose the measured signal into IMFs, in a sequence from the highest frequency component to the lowest frequency component. The standard EMD algorithm is summarized in Table I. The steps 1 to 5 are known as sifting process.

TABLE I
Standard EMD algorithm.

Step 0: Set $n=1$; $r(t)=y_i(t)$;
Step 1: Identify the local maxima and minima in $r(t)$;
Step 2: Calculate the upper envelope defined by the maxima, and the lower envelope defined by the minima;
Step 3: Calculate the mean envelope $m(t)$;
Step 4: Set $h(t)=r(t) - m(t)$;
Step 5: If $h(t)$ is an IMF, go to next step. Otherwise, set $r(t)=h(t)$ and go back to step 1;
Step 6: Set $c_{n,i}(t)=h(t)$; $r(t)=r(t) - c_{n,i}(t)$;
Step 7: If $n=N$, define the IMF components as $c_{1,i}(t), \ldots, c_{N,i}(t)$, and the residue as $r_{N,i}(t) = r(t)$. Otherwise, set $n=n+1$ and go back to step 1.

In the standard EMD algorithm, the sifting iterations are performed in the full length of the signal. Thus, the knowledge of the whole signal (or previous residual) is needed to extract a mode, which would cause excessively long delays, impractical in the estimation of WF motions for real-time applications. Nonetheless, an online version of the method is based on the observation that the sifting process relies on interpolations between a finite number of extrema, and then, the extraction of a mode is done blockwise by means of a sliding window [13]. In such a case, the knowledge of the whole signal is not needed, but some delay is also observed as the sifting process requires a certain number of extrema to extract a meaningful IMF (10 extrema in the case of cubic splines) [13]. The online EMD algorithm considered in this study is presented next.

B. Online EMD

In the online EMD algorithm, the fastest mode is extracted by using the sifting process in the standard EMD at each instant in which a sliding window contains a specified number of local extrema (l). The mode is updated (as the window shifts by one extremum) through a stitching procedure that weights and averages overlapping modes according to their position in time [9]. After obtaining the first IMF, the procedure is repeated using the residual of the signal to identify other IMFs. The online EMD algorithm is summarized in Table II for the extraction of an IMF $c_{n,i}(t)$ from the input signal $x(t)$, which is defined as $x(t) = y_i(t)$ for the first IMF ($n = 1$) or $x(t) = r_{n,i}(t)$ for subsequent IMFs.

The section of the IMF that is being stitched needs subsequent data to be completed and will exhibit a time lag that

TABLE II
ONLINE EMD ALGORITHM [9]

Step 0: Set $m=1$; $\Phi^0(t)=0$; $e_1=0$; $\bar{c}_{n,i}=0$;
Step 1: Identify the window with l consecutive local extrema ($\{e_1,\ldots,e_l\}$) in $x(t)$;
Step 2: Extract an IMF $c^m_{n,i}(t)$ for the data in the window m using the standard EMD (sifting process);
Step 3: Define warped weights as: $\phi_k(t)=\begin{cases}\tilde{\phi}\left(s_k+(s_{k+1}-s_k)\frac{t-e'_k}{e'_{k+1}-e'_k}\right), t\in[e'_k,e'_{k+1}]\\ 0\,, \text{otherwise}\end{cases}$ and the weighted IMF as: $\hat{c}^m_{n,i}(t)=(\phi_1(t)c^{m,1}_{n,i}(t),\ldots,\phi_{l'-1}(t)c^{m,,l'-1}_{n,i}(t))$, where e'_k is the position of the k-th extremum in $c^m_{n,i}(t)$, $\tilde{\phi}$ is the window function: $\tilde{\phi}(s)=\begin{cases}\frac{1}{\sqrt{2\pi}}\exp\left(-\frac{s^2}{2}\right)-\frac{1}{\sqrt{2\pi}}\exp\left(-\frac{\tau^2}{2}\right), \text{on } [-\tau,\tau]\,,\\ 0\,, \text{otherwise}\end{cases}$ $s_k=-\tau+2(k-1)\tau/(l'-1)$, and $c^{m,k}_{n,i}(t)$ is the mode between two extrema: $c^{m,k}_{n,i}(t)=c^m_{n,i}(t)$, $e'_k\le t<e'_{k+1}$. Store the total of weights: $\Phi^m=\Phi^{m-1}(t)+\sum_{k=1}^{l'-1}\phi_k(t)$;
Step 4: Stitch $\hat{c}^m_{n,i}(t)$ on weighted IMFs previously extracted: $\bar{c}_{n,i}(t)=\bar{c}_{n,i}(t)+\hat{c}^m_{n,i}(t)$ and normalize the data that will be removed from the sliding window in the next iteration: $\bar{c}_{n,i}(t)=\bar{c}_{n,i}(t)/\Phi^m(t)$, for all $t\in[e_m,e_{m+1}]$;
Step 5: Update the residual: $r^m_{n,i}(t)=x^m(t)-\bar{c}_{n,i}(t)$ for all $t\in[e_m,e_{m+1}]$;
Step 6: Set $m=m+1$ and go back to step 1.

depends on the distance between the extrema [9]. Then, each IMF has a lag determined by the frequency of its waveform, and IMFs with low frequencies have longer delays than high-frequency IMFs.

Here, the aim is to estimate the time needed to obtain the high-frequency induced motions by using the online EMD. Thus, the lag of the last IMF $c_{N,i}(t)$ in (15)-(17) is of interest.

C. Performance Metrics

To evaluate the performance of the EMD, the following metrics are adopted: (i) the mean square error (MSE) between the LF motions and the desired Earth-fixed frame position and heading $\boldsymbol{\eta}_d=[\mathcal{N}_d,\mathcal{E}_d,\psi_d]^T$; (ii) the MSE of WF motions obtained with the online EMD and standard EMD; and (iii) control effort metrics ($J_{\tau,\mathrm{uv}}$, $J_{\tau,\mathrm{r}}$) to verify the control action required when the EMD method is used for wave filtering:

$$J_{\tau,\mathrm{uv}} = \int_0^T \left(|\tau_{\mathrm{surge}}|+|\tau_{\mathrm{sway}}|\right)\,dt\,, \tag{18}$$

$$J_{\tau,\mathrm{r}} = \int_0^T |\tau_{\mathrm{yaw}}|\,dt\,, \tag{19}$$

where T is a time interval. Furthermore, the time lag of the last IMF for each motion is of interest in the online EMD, as it indicates the WF prediction time window.

IV. SIMULATION RESULTS

In order to evaluate the performance of the EMD method in terms of wave filtering and control effort metrics, a comparison with the NPO is performed in this section.

TABLE III
SEA STATES

Sea state	ω_p (rad/s)	H_s (m)
Calm sea	1.11	0.2
Moderate sea	0.79	2

TABLE IV
MAIN PARAMETERS OF THE SUPPLY VESSEL

Parameter	Value
Length between perpendiculars	59.13 m
Breadth	13.11 m
Design draft	4.59 m
Mass	2067 tons

TABLE V
DEFINITION OF WAVE FILTERING METHODS USED IN SIMULATIONS

Method	Definiton
M0	NPO
M1	EMD with $N=1$
M2	EMD with $N=2$
M3	EMD with $N=3$

A. Simulation parameters

The simulations were performed using building blocks from the Marine Systems Simulator (MSS) [14] to model the motions of a platform supply vessel with a nonlinear PID control. The simulation model adopts high-fidelity model formulations, as presented in [10, Section 3], but only the forces and moments due to waves and control are considered here. The vessel is subject to waves from both calm and moderate seas. Table III shows the significant wave height (H_s) and peak frequency (ω_p) for JONSWAP spectra adopted in the simulations, and Table IV shows the main parameters of the supply vessel. The gains of the nonlinear PID and NPO were adjusted using the tuning rules as presented in [11]. Here, $K_{3i}=0.01$, $K_{4i}=0.1$, $T_{bi}=1000$, $\zeta_i=0.05$, $\zeta_{ni}=1.0$, $\omega_{oi}=\omega_p$, and $\omega_{ci}=1.22\omega_{oi}$.

For the EMD method (both standard and online algorithms), different wave filtering characteristics are considered in the analysis, i.e., the WF motions are defined using distinct numbers of IMFs. Table V summarizes the wave filtering methods used in the simulations. The EMD algorithms apply 10 sifting iterations to extract the modes in all studied cases. The online EMD from [9] is used in the simulations. The same wave conditions and controller gains are considered for all methods in Table V.

B. Standard EMD

Firstly, we adopt the standard EMD to estimate the WF motions of the vessel in a station keeping scenario, where the controller regulates the position and heading of the vessel around zero. Figure 1.a illustrates the measured position in East (top), and the IMFs and residue obtained from the

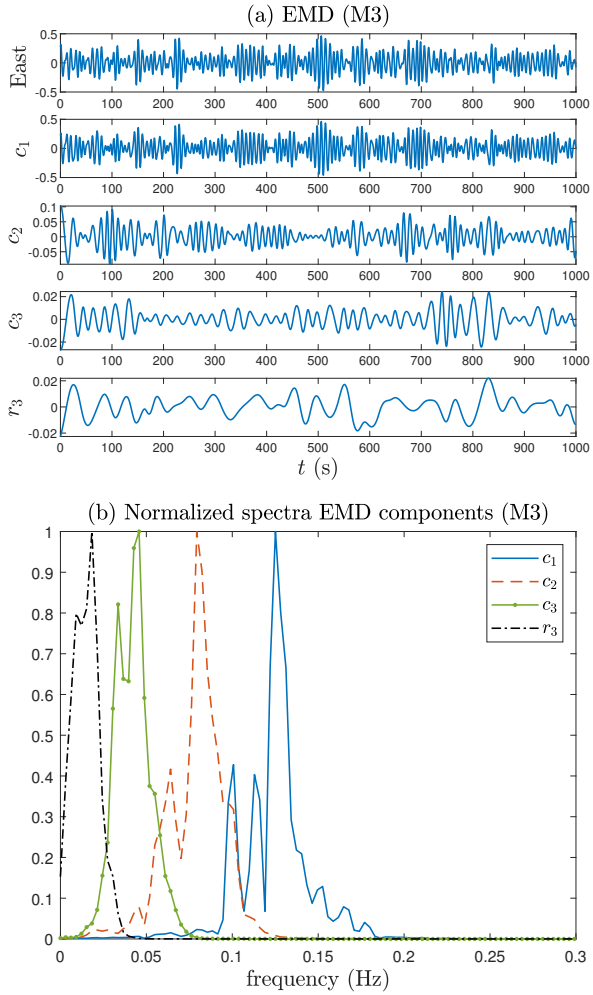

Fig. 1. Standard EMD (M3) applied in measured position of the vessel in moderate sea: (a) measured signal (top) and EMD components, (b) normalized spectra of EMD components. East in meters. Index $i=2$ is omitted in labels and legend.

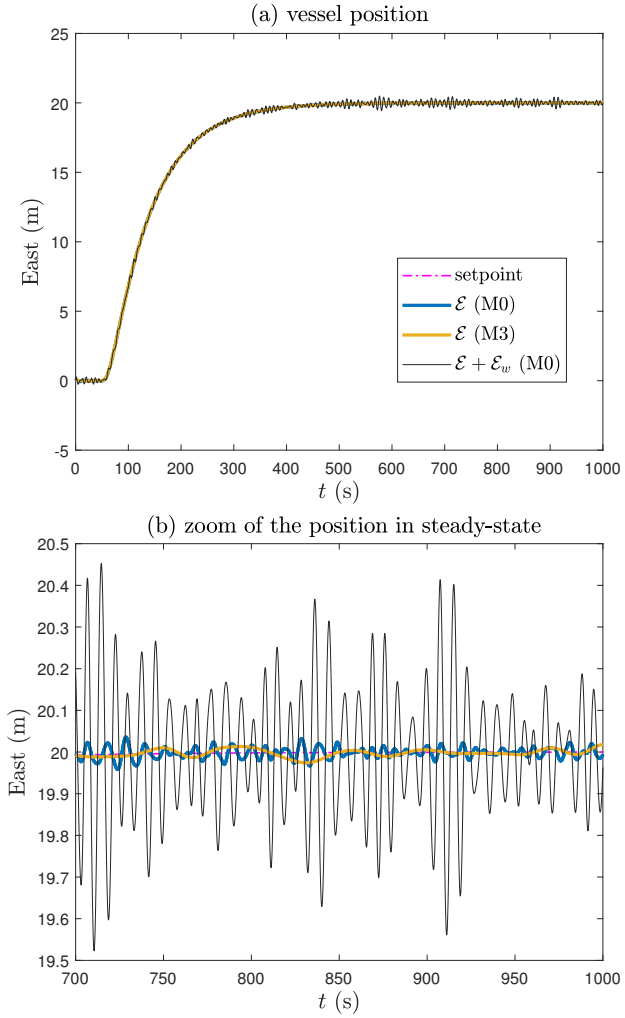

Fig. 2. Setpoint, total motion, and LF components for methods M0 and M3 for a test maneuver in moderate sea: (a) vessel position, (b) zoom of the position in steady-state.

decomposition when $N = 3$ (M3) for moderate sea. The normalized spectra of the IMFs and residue are shown in Figure 1.b.

It can be noted the peak frequencies of the IMFs are distinct, and the peak frequency ratio for neighbouring spectra is roughly 2, but there is overlapping in sub-bands of the spectra. As discussed in [15], the EMD acts as a filter bank structure, where the filter for the first mode is essentially high-pass, and a set of overlapping band-pass filters characterize subsequent modes. The peak frequencies of the IMFs (Fig. 1.b) are within the frequency range (1), and for M3, the estimated WF component for each degree of freedom i is the superposition of $c_{1,i}(t)$, $c_{2,i}(t)$ and $c_{3,i}(t)$.

Figure 2 illustrates a simple maneuver of the vessel, when its position is commanded to move 20 m sideways in sway while keeping the surge and heading at zero by using methods M0 and M3 for wave filtering. The total motion ($\mathcal{E} + \mathcal{E}_w$) and the set-point are also shown. It can be noted that M3 provides better filtering than M0. However, the drawback of M3 is that the WF motions are estimated in advance, while M0 is a model-based method that only requires the information of the dominant frequency for estimating the current WF components.

The sway control force, and the normalized control effort metrics, are shown in Figure 3 for the test maneuver. The control effort metrics are normalized to the maximum values obtained with M0. The control effort metrics $J_{\tau,\mathrm{uv}}$, and $J_{\tau,\mathrm{r}}$, with method M3 are about 35%, and 45%, lower than the metrics when M0 is used for wave filtering. Such a decrease in the control effort metrics can reduce the fuel consumption.

Tables VI and VII summarize the performance metrics, i.e, the MSE of LF components and the control effort metrics, for all methods in Table V in moderate sea, and calm sea, respectively. The results obtained for M1 are inferior since it filters only part of the high-frequency wave induced motions with the first IMF (as illustrated in the IMFs spectra in Fig. 1.b). Nevertheless, M2 covers a wider frequency bandwidth than M1, and it results in control effort metrics lower than M0

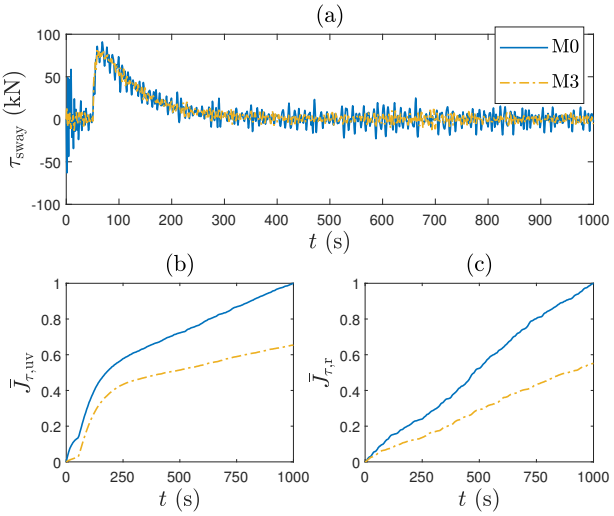

Fig. 3. Control performance with methods M0 and M3 (a) sway force (b) normalized effort metric $\bar{J}_{\tau,\text{uv}}$, (c) normalized effort metric $\bar{J}_{\tau,\text{r}}$.

TABLE VI
NORMALIZED CONTROL EFFORT METRICS ($\bar{J}_{\tau,\text{uv}}$, $\bar{J}_{\tau,\text{r}}$) AND MSE [LF] IN MODERATE SEA. METHODS M1-M3 WITH STANDARD EMD. TIME INTERVAL: $T=1000$S.

Method	Control effort metrics		MSE [LF]		
	$J_{\tau,\text{uv}}$	$J_{\tau,\text{r}}$	North	East	Heading
M0	1.00	1.00	9.6×10^{-4}	3.7×10^{-4}	9.0×10^{-7}
M1	3.25	2.41	2.4×10^{-3}	1.2×10^{-3}	4.5×10^{-7}
M2	0.73	0.88	1.7×10^{-4}	1.5×10^{-4}	3.8×10^{-7}
M3	0.65	0.55	0.6×10^{-4}	0.6×10^{-4}	1.2×10^{-7}

TABLE VII
NORMALIZED CONTROL EFFORT METRICS ($\bar{J}_{\tau,\text{uv}}$, $\bar{J}_{\tau,\text{r}}$) AND MSE [LF] IN CALM SEA. METHODS M1-M3 WITH STANDARD EMD. TIME INTERVAL: $T=1000$S.

Method	Control effort metrics		MSE [LF]		
	$J_{\tau,\text{uv}}$	$J_{\tau,\text{r}}$	North	East	Heading
M0	1.00	1.00	2.3×10^{-6}	4.3×10^{-6}	2.3×10^{-8}
M1	1.36	1.92	3.6×10^{-6}	3.3×10^{-6}	0.4×10^{-8}
M2	0.99	0.87	0.3×10^{-6}	0.5×10^{-6}	0.3×10^{-8}
M3	0.98	0.60	0.1×10^{-6}	0.4×10^{-6}	0.2×10^{-8}

for both moderate and calm seas. For M0, a notch effect is obtained in the peak frequency ($\omega_p = 0.79$ rad/s) and the observer acts a low-pass filter for frequencies higher than the cutoff frequency ($\omega_{ci} = 0.96$ rad/s), as discussed in [11, Chapter 11]. For the metric $J_{\tau,\text{uv}}$, the reductions observed with M2, and M3, in calm sea are less significant than in moderate sea. The MSEs of LF components with M2, and M3, are also lower when compared to the MSE with M0.

C. Online EMD

We consider the same wave-forms as used in the standard EMD, in order to compare the results obtained with both methods. Figure 4 illustrates the IMFs and WF motions (bottom) obtained from the online decomposition with $N=3$ (M3) and window length $l=10$ in moderate sea. The red parts

TABLE VIII
NORMALIZED CONTROL EFFORT METRICS ($\bar{J}_{\tau,\text{uv}}$, $\bar{J}_{\tau,\text{r}}$) AND MSE [LF] IN MODERATE SEA. METHODS M2 AND M3 WITH ONLINE EMD AND $l=10$. TIME INTERVAL: $T=900.7$S (M2), AND $T=802.4$S (M3).

Method	Control effort metrics		MSE [LF]		
	$\bar{J}_{\tau,\text{uv}}$	$\bar{J}_{\tau,\text{r}}$	North	East	Heading
M2	0.79	0.62	1.6×10^{-4}	1.3×10^{-4}	9.6×10^{-6}
M3	0.67	0.60	0.6×10^{-6}	0.6×10^{-4}	1.7×10^{-6}

in each IMF highlight the sections that are not yet completed due to the stitching procedure. Such sections indicate the lag of each IMF, which is determined by the frequency of the IMF. Thus, $c_{3,i}(t)$ has a longer lag than previous IMFs since its frequency is lower. Here, the lag of the last IMF for each motion is of interest. From Figure 4, the longest lag is around 200 s and this indicates the WF prediction time for M3. Furthermore, the lag of $c_2(t)$ for the sway motion ($i=2$) is around 100 s, and this is the WF prediction time for M2.

Table VIII summarizes the performance metrics for methods M2, and M3, when the online EMD is adopted with a window length of $l=10$ in moderate sea. The control effort metrics are normalized to the maximum values obtained with M0. It can be noted that the metrics are in agreement with the metrics obtained with the standard EMD (Table VI). The advantage of using the online algorithm is the possibility of decomposing data flows, which is more suitable for real-time applications.

In order to illustrate the effect of the window length (i.e., the number of extrema) on the estimated WF motions, Figure 5 shows the MSE of WF motions, and the WF prediction time $\Delta\mathcal{T}$ as a function of the window length. Different numbers of extrema (from 3 to 10) are adopted in the online algorithm with M2, and M3. As expected, the WF prediction time reduces with the window length ($\Delta\mathcal{T}$ is around 15s for M2 with $l=3$). However, due to errors introduced by the stitching procedure, the MSE of WF motions increases as the window length reduces. Therefore, further studies are needed to improve the decomposition for shorter WF prediction time.

V. CONCLUSIONS

This paper evaluated the use of the empirical mode decomposition method for wave filtering purposes in DP systems. Simulation results with a simple maneuver of a vessel indicate that as the wave height increases, the benefit of applying EMD for wave filtering purposes in DP systems can be significant, since the control action is further reduced when compared to the nonlinear passive observer, a more conventional method in DP systems. In contrast to NPO, which is based on simplified models that do not accurately describe the real vessel wave-frequency dynamics, EMD is a non-model based approach with an adaptive basis that relies on the local characteristic time-scale of the vessel motions. However, as it is suggested by the name of the method, EMD is essentially an empirical method that lacks a solid theoretical foundation. Thus, it does not allow an analysis of its stability properties.

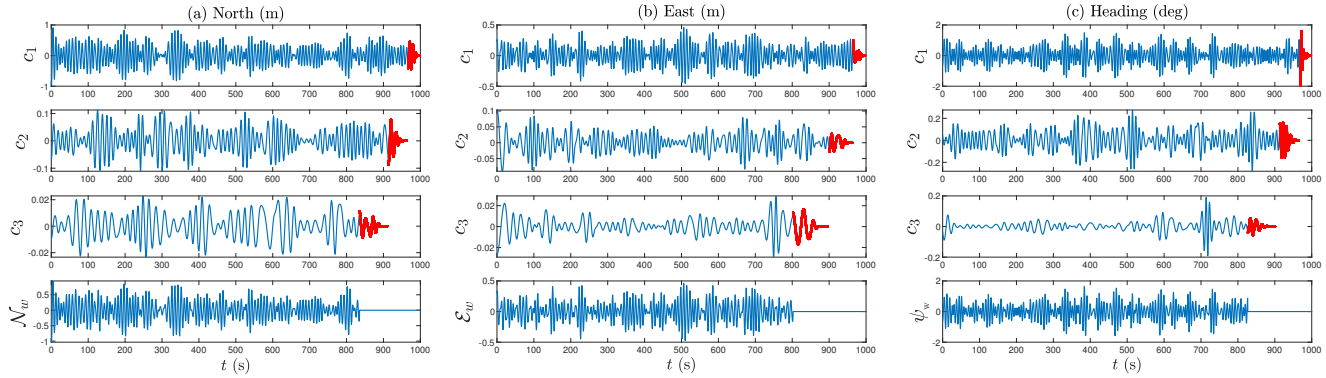

Fig. 4. Online EMD (M3) with window length $l = 10$ applied in measured position and heading of the vessel in moderate sea. Index i is omitted in IMF labels.

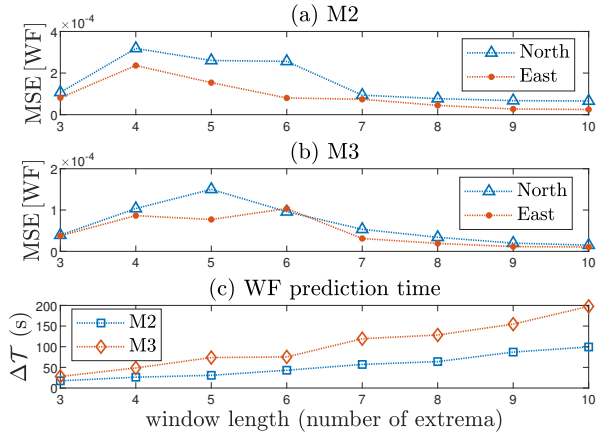

Fig. 5. WF characteristics for the online EMD. (a) MSE with method M2, (b) MSE with method M3, (c) prediction time window with methods M2 and M3.

Furthermore, high-frequency motions obtained with the online EMD feature a time lag. Therefore, measurements of the vessel position and heading have to be taken at a point ahead of the center of gravity to allow the estimation of high-frequency induced motions in advance. The wave-frequency prediction time is a function of the length of the sliding window, number of IMFs to ensure proper wave filtering and the frequencies of such IMFs, and number of sifting iterations (kept fixed as 10 in this study). For the studied cases, the wave-frequency prediction time is of the order of minutes, around 100s to 200s, depending on the wave filtering properties adopted. This time window of prediction is too long for DP real-time applications. Further studies are needed to improve the online EMD decomposition for smaller sliding window lengths, and then, decrease the prediction time window for estimating high-frequency motions in DP systems.

References

[1] T. I. Fossen, *Guidance and Control of Ocean Vehicle*. Wiley, 1994.

[2] T. I. Fossen and J. P. Strand, "Passive nonlinear observer design for ships using Lyapunov methods: full-scale experiments with a supply vessel," *Automatica*, vol. 35, no. 1, pp. 3–16, 1999.

[3] J. G. Balchen, N. A. Jenssen, E. Mathisen, and S. Saelid, "Dynamic positioning of floating vessles based on Kalman filtering and optimal control," in *19th IEEE Conference on Decision and Control*, Albuquerque, USA, 1980, pp. 852–864.

[4] G. Torsetnes, J. Jouffroy, and T. I. Fossen, "Nonlinear dynamic positioning of ships with gain-scheduled wave filtering," in *Proc. of the 43rd IEEE Conference on Decision and Control*, Nassau, Bahamas, 2004, pp. 5340–5347.

[5] T. I. Fossen and T. Perez, "Kalman filtering for positioning and heading control of ships and offshore rigs," *IEEE Control Systems Magazine*, vol. 29, no. 6, pp. 32–46, 2009.

[6] V. Hassani, A. J. Sørensen, and A. M. Pascoal, "Adaptive wave filtering for dynamic positioning of marine vessels using maximum likelihood identification: Theory and experiments," in *Proc. of the 9th IFAC Conference on Control Applications in Marine Systems*, vol. 46, no. 33, Osaka, Japan, 2013, pp. 203–208.

[7] M. Loueipour, M. Keshmiri, M. Danesh, and M. Mojiri, "Wave filtering and state estimation in dynamic positioning of marine vessels using position measurement," *IEEE Transactions on Instrumentation and Measurement*, vol. 64, no. 12, pp. 3253–3261, 2015.

[8] N. E. Huang, Z. Shen, S. R. Long, M. C. Wu, H. H. Shih, Q. Zheng, N.-C. Yen, C. C. Tung, and H. H. Liu, "The empirical mode decomposition and the Hilbert spectrum for nonlinear and non-stationary time series analysis," *Proc. Royal Society London*, vol. 454, pp. 903–995, 1998.

[9] R. Fontugne, P. Borgnat, and P. Flandrin, "Online empirical mode decomposition," in *Proc. of the IEEE International Conference on Acoustics, Speech and Signal Processing (ICASSP)*, New Orleans, USA, 2017, pp. 4306–4310.

[10] A. J. Sørensen, "A survey of dynamic positioning control systems," *Annual Reviews in Control*, vol. 35, no. 1, pp. 123–136, 2011.

[11] T. I. Fossen, *Handbook of marine craft hydrodyamics and motion control*. Wiley, 2011.

[12] Z. Wu and N. E. Huang, "A study of the characteristics of white noise using the empirical mode decomposition method," *Proc. Royal Society London*, vol. 460, pp. 1597–1611, 2004.

[13] G. Rilling, P. Flandrin, and P. Gonçalves, "On empirical mode decomposition and its algorithms," in *Proc. of the IEEE-EURASIP Workshop on Nonlinear Signal and Image Processing NSIP-03*, Grado, Italy, 2003.

[14] T. I. Fossen and T. P. (2004), "Marine systems simulator (MSS)," https://github.com/cybergalactic/MSS.

[15] P. Flandrin, G. Rilling, and P. Gonçalves, "Empirical mode decomposition as a filter bank," *IEEE Signal Processing Letters*, vol. 11, no. 2, pp. 112–114, 2004.